Thin Casein Films as Prepared by Spin-Coating: Influence of Film Thickness and of pH

P. Müller-Buschbaum,*,† R. Gebhardt,† E. Maurer,† E. Bauer,† R. Gehrke,‡ and W. Doster†

TU München, Physik-Department, LS E13, James-Franck-Str.1, 85747 Garching Germany, and HASYLAB at DESY, Notkestr. 85, 22603 Hamburg, Germany

Received January 30, 2006; Revised Manuscript Received March 22, 2006

Casein films were successfully prepared with the spin-coating technique of aqueous casein solutions on base-treated glass surfaces. The film structure is investigated in real space with optical microscopy and atomic force microscopy and for the first time in reciprocal space with grazing incidence small-angle X-ray scattering (GISAXS). The size of the substructures detected in the film increases with pH from 170 nm (pH 5.1) up to 490 nm (pH 9.4). Dynamic light scattering experiments reveal that the average diameters of casein micelles in solution exhibit the same quantitative increase. This result suggests that the substructures detected in the bulklike films with GISAXS reflect intact casein micelles. However, with thin homogeneous casein films, the micelle size diminishes with decreasing film thickness. This indicates that the moderate pressures introduced by spin-coating force the micelles to rearrange into a more compact structure.

Introduction

Caseins represent about 80% of the proteins in milk. Technically, caseins are applied in adhesives, binders, protective coatings, and other products. The principal casein fractions are α-(*s*1)- and α-(*s*2)-caseins, *β*-casein, and *κ*-casein.[1] A common property of all caseins is their low solubility at low pH (4.6, isoelectric point). Caseins are conjugated proteins, mostly with phosphate group(s) esterified to serine residues. Calcium binding by the individual caseins is proportional to the phosphate content. The conformation of caseins resembles those of denatured globular proteins. The large number of proline residues in caseins causes particular bending of the protein chain and inhibits the formation of closely packed secondary structures. Because of the lack of secondary structure, hydrophobic residues result in strong association reactions of the casein monomers and render them insoluble in water. The casein proteins arrange with calcium phosphate into a superstructure known as the casein micelle (α-(*s*1)- and α-(*s*2)-caseins, *β*-casein, and *κ*-casein in the weight ratio 3:0.8:3:1). Its biological function is to carry large amounts of highly insoluble calcium phosphate ($Ca_3(PO_4)_2$; denoted CaP). Besides casein protein, calcium, and phosphate, the micelle also contains citrate, minor ions, lipase and plasmin enzymes, and entrapped milk serum. These micelles are rather porous structures, occupying about 4 mL/g and 6−12% of the total volume fraction of milk.

Despite the numerous X-ray and neutron scattering experiments,[2−8] the micellar substructure is still under debate.[9] In a submicelle model, the presence of smaller subunits is suggested,[10−12] and alternatively, a dual binding model invokes a description analogous to diblock copolymers.[13,14] Other models do not assume submicelles and consider instead CaP clusters as centers of micelle growth.[2] However, with respect to applications, the size and the distance between casein micelles is of interest. Because the typical size of micelles is on the order of 100 nm,[15] these experiments, addressing the mesoscopic structure, require a high resolution, which is, for example, available under ultrasmall-angle scattering conditions.[6]

Whereas most investigations address solutions at different casein concentrations, in the most prominent applications besides milk, films containing caseins are used: (1) Paint, which may be diluted with water and is useable on most surfaces, consists of casein, as do (2) adhesives for labeling of glass containers, making use of the advantage of a high initial tack, high wet strength, and easy removal in the bottle washer. In these typical applications, casein films are prepared with solution-casting or spray-coating equivalent techniques.[16] Completely unexplored is a thin film preparation with the spin-coating technique. Spin-coating is a largely used process for the preparation of thin and ultrathin films out of synthetic polymers.[17−19] Depending on the (synthetic) polymer/solvent combination films with a very high quality in terms of homogeneity, thickness uniformity and small surface roughness can be obtained.[20] Because it is controlled by the preparation parameters, the film thickness can be varied in a wide range from the submonolayer regime up to several microns (bulklike films). However, because of the complex nature of the spin-coating process, major simplifying assumptions have been used, and thus, the successful modeling is restricted to a few homopolymer systems.

Because of the importance in technical applications such as photoresist films in the semiconductor industry and protective coatings in microelectronics and optics, spin-coating is experimentally well investigated for synthetic polymers. Important parameters, besides the actual spinning parameters used for the process, are polymer concentration, viscosity, and molecular weight, which determine the final film thickness.[21,22]

Within this investigation, we focus on the possibility of preparing thin casein films via spin-coating. Concentration and pH value of the casein solution are selected control parameters, showing strong effect on the spin-coating (concentration) and casein micelle size (pH value).[23−25] With spin-coating, new aspects of an advanced casein thin film preparation will become accessible. Moreover, a comparison with the well-investigated bulk structure is included.

After a short introduction to the experimental methods, grazing incidence small-angle X-ray scattering, atomic force microscopy, and dynamic light scattering, the influence of pH

† TU München.
‡ HASYLAB at DESY.

10.1021/bm060088u CCC: $33.50
Published on Web 05/17/2006

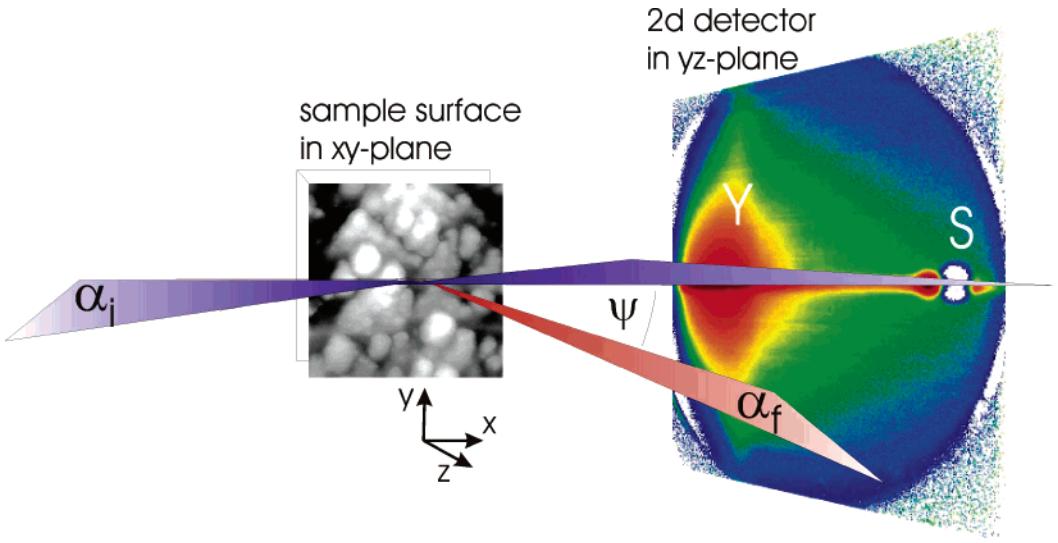

Figure 1. Schematic top view of the GISAXS geometry making use of a two-dimensional detector in the *yz*-plane to picture the scattering geometry. The sample is placed in the *xy*-plane and consists of a casein film. The incident angle is denoted α_i and the exit angle α_f. The structural information is obtained from a *y*-cutout of the two-dimensional intensity distribution perpendicular to the scattering plane (*xz*-plane) indicated by the two opposite triangles. The GISAXS signal is probed as a function of the out-of-plane angle ψ. As figuratively shown, the diffusely scattered intensity in the scattering plane exhibits a Yoneda peak (Y) and a specular peak (S) as common features.

for a fixed film thickness and the influence of film thickness for a fixed pH value are discussed. A summary concludes the paper.

Experimental Section

Sample Preparation. Casein films were prepared by spin-coating (2000 rpm, 30 s) onto precleaned glass slides.[17−19] For cleaning, the glass slides were placed in dichloromethane in an ultrasonic bath for 5 min and rinsed with Millipore water shortly after. Afterward, the glass substrates were kept for 2 h in an oxidation bath at 75 °C consisting of 1400 mL Millipore water, 120 mL H_2O_2, and 120 mL NH_3 to clean the surface from organic traces. Thereafter, the samples were stored in Millipore water. Directly before spin-coating, the glass slides were rinsed with Millipore water at least 5 times to remove possible traces of the oxidation bath. The samples were dried using compressed nitrogen before coating the glass surface.

Extracted casein micelles of a desired concentration were dissolved in purified water. Extraction was made from commercial-grade skim milk by a combined uniform transmembrane pressure microfiltration (mean pore diameter 0.1 μm) and ultrafiltration, followed by 5 washing steps and drying in a spray tower.[26] The pH of the solution was adjusted by using a buffer solution. A pH range from 5.15 to 9.35 was addressed. Below pH of 7.0, a buffer based on filtered 0.1 M Mes/Tris−HCl solution was used, and above, filtered 0.1 M Tris−HCl buffer solution was added. No additional Ca (but within a dilution series purified water was used) was put in to change the concentration used for the film preparation. Starting with 100 g/L on an exponential scale, the concentration was reduced down to 0.32 g/L. All solutions were equilibrated by thoroughly stirring for 5 h at 20 °C.

The samples were freshly prepared in advance of the scattering experiment. Dry films were investigated resembling the final state being present in applications.

Dynamic Light Scattering. The dynamic light scattering spectrometer with goniometer and monomode fiber detection (ALV−Laser GmbH, Langen) is equipped with two lasers: a 22 mW HeNe laser at 632 nm (JDS Mod. 1145P) and a 150 mW frequency doubled Nd:YAG laser at 532 nm (Coherent DPSS 532−150). The correlation function of the scattered intensity was calculated using an ALV-5000 correlator on a logarithmic time scale ranging from 10 ns to 10 s. The dynamic light scattering (DLS) experiments were performed with casein solutions at concentrations matching exactly those used for the spin-coating technique. A backscattering geometry was selected to probe turbid casein solutions. Data of transparent solutions were collected at scattering angles Θ between 30 and 177, which correspond to scattering wave vectors $2.7 \times 10^{-3} < q < 3.2 \times 10^{-2}$ nm^{-1} with $q = [4\pi n \sin(\Theta/2)]/\lambda$. Here, n denotes the refractive index and λ the laser wavelength. The temperature was controlled by a thermostat bath and was set at 20 °C.

Optical Investigation. The sample surfaces were observed with optical microscopy using a Zeiss Axiotech 25H optical microscope with magnifications between 4× and 100×. A Hitachi KP-D50 CCD camera recorded the micrographs.

X-ray Off-Specular Scattering. Grazing incidence small-angle X-ray scattering (GISAXS) offers an opportunity to address large-scale structures in thin films.[27−29] By replacing the common transmission with a reflection geometry, surface sensitivity is achieved. The GISAXS experiments were performed at the BW4 beamline at the synchrotron HASYLAB (DESY, Hamburg). The selected wavelength was $\lambda = 0.138$ nm. For further details concerning the beamline, see ref 30. A setup of high-quality entrance slits and a completely evacuated pathway was used. The two entrance cross-slits defined the beam divergence in and out of the plane of reflection to match the detector resolution. A sample−detector distance of 12.8 m allowed a high-resolution experiment, and a resolution better than $1.42 \cdot 10^{-3}$ nm^{-1} was achieved. Consequently, the setup accessed lateral lengths from 35 nm up to 4400 nm. A beam-stop in front of the detector was installed at the position of the specular peak to shield the detector. At one fixed angle of incidence $\alpha_i = 0.6451°$, the two-dimensional intensity distribution was recorded with a two-dimensional detector consisting of a 512 × 512 pixel array. A schematic picture of the setup used is shown in Figure 1. A detailed description of GISAXS as an advanced scattering technique for the investigation of nanostructured polymer films is given in ref 29. The two-dimensional intensity distribution can be understood as an assembly of several vertical and horizontal slices.[27]

The sample surface is defined as the (*x*, *y*)-plane. The incident beam is directed along the *x*-axis with an incident angle α_i. The (*x*, *z*)-plane denotes the plane of incidence and reflection, and thus, the condition for specular scattering is given by $q_x = q_y = 0$ and $q_z > 0$, with the scattering vector $\vec{q} = (q_x, q_y, q_z)$.[31] The specular peak fulfills the specular condition ($\alpha_i = \alpha_f$). Diffusely scattered intensity is observed for $q_x \neq 0$ or $q_y \neq 0$.[31] Consequently, the two-dimensional detector (see Figure 1) basically contains diffusely scattered information. GISAXS is

observed along the out-of plane direction and satisfies the condition $q_y \neq 0$.[28]

In case of small roughnesses (with $|q_z|^2 C(\mathbf{R})| \ll 1$), which is commonly fulfilled for nanostructured polymer surfaces, the GISAXS signal is directly proportional to the diffuse scattering factor

$$S(\mathbf{q}) = \frac{\Delta\rho^2}{|q_z|^2} e^{-[q_z^2+(q_z^*)^2]\sigma^2/2} |q_z|^2 \int\int C(\mathbf{R}) \exp(-\imath \mathbf{q}_\parallel \mathbf{R})\, d\mathbf{R} \quad (1)$$

with the density contrast $\Delta\rho$ and the rms surface roughness σ. Thus, the GISAXS signal is directly proportional to the Fourier transform of the height-height correlation function $C(\mathbf{R})$ of the effective surface.[27] Thus, the shape of the GISAXS signal is affected by changes in the characteristic length sales such as shape and distances between scattering particles (e.g., the casein micelles). It is observable in *y*-cuts (horizontal) of the 2D intensity distribution (see Figure 1). To improve the statistics, a slab in *q*-space with a width of $\Delta q_z = \pm 3.8 \cdot 10^{-3}$ nm^{-1} was integrated.

Atomic Force Microscopy. Using a PARK Autoprobe CP atomic force microscope, the sample surface is probed. All measurements were performed in air at room temperature. The amplitude of the oscillation of the tip was calibrated with respect to the vertical position of the piezoelectric scanner. The distance calibration of the piezocontroller was performed with a standard gold grating. Each scanned micrograph consists of 265 lines, scanned with 0.25 Hz up to 1.0 Hz. Several images were measured for each sample. Micrographs were recorded at different sample positions. Contact avoidance to the sample minimized the tip-induced sample degradation. The silicon gold-coated conical cantilevers had resonant frequencies at about $f = 60$ kHz and a spring constant of approximately 2.1 N m^{-1}. At each individual sample position, scans with different ranges from 1 μm × 1 μm up to 10 μm × 10 μm were performed. From the raw data, the background due to the scanner tube movement was fully subtracted to determine the values of the rms roughness over the complete scan area.

Results and Discussion

As worked out for synthetic polymers, the spin-coating process can be subdivided into three different stages:[17−19] First, a casein solution with a low concentration is dropped onto the substrate, which is started to spin. During the initial stages, most of the solution is cast off, leaving a thin layer on the substrate. As the layer thins due to fluid flow, the evaporation of the solvent becomes important. The evaporation increases the viscosity of the casein solution and slows the shear thinning of the film. Solvent evaporation freezes in the developing surface structure. For blends of synthetic polymers, it is well-known that spin-coating initiates nonequilibrium structures and thereby enlarges the range of accessible structures.[33−35] Depending on the stage at which the structure is installed, two major types can be distinguished: (1) isotropic surface patterns, whose typical characteristics do not depend on the position on the substrate with respect to the center of rotation of the spinning, and (2) anisotropic surface patterns, which, due to flow, exhibit a change with increasing distance from the center of rotation.[36] Moreover, not all solutions are useable for spin-coating, and the attempt to create homogeneous films might fail completely.[37]

So, with respect to water-based casein solutions, questions arise whether homogeneous casein films are obtainable at all and whether the resulting structures belong to type 1 or type 2 as explained above. In addition, casein micelles, which are stabilized in aqueous suspension by steric and electrostatic repulsion between the layers of κ-caseins around the micelles[38] and which are in dynamic equilibrium with smaller aggregates and monomers,[11] might remain unchanged by the spin-coating. The integrity of the micelle, which is kept by minerals, constituting 7% of the dry weight of the micelle and mainly existing as colloidal calcium phosphate (CCP), might be lost due to the forces involved in spin-coating.

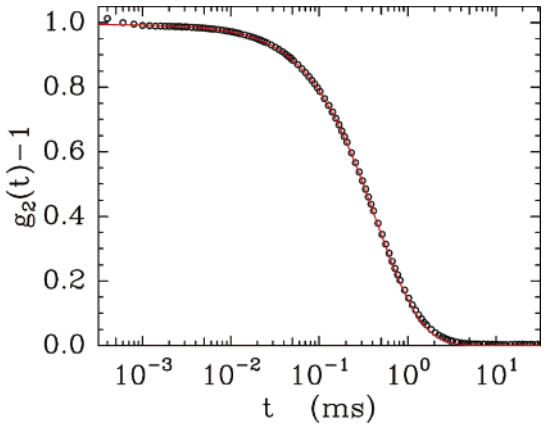

Figure 2. Measured (circles) normalized time autocorrelation function of the intensity $g_2(t)$ as a function of time t in the case of pH = 7.8 in backscattering geometry (177°), shown together with a fit calculated from the radial size distribution.

1. Influence of pH on Structure. For comparison with the structures obtained in the prepared films, bulk solutions are probed with dynamic light scattering (DLS). The DLS experiments were performed at highly concentrated (100 g/L) casein solutions matching exactly those used for the spin-coating. With photon correlation spectroscopy (PCS), the correlation function of the intensity fluctuations versus time, which depends on Brownian diffusion of the particles, is determined. For a single species with diffusion coefficient D, the normalized time autocorrelation function of the intensity is given by[39]

$$g_2(t) = \frac{\langle I(0)I(t)\rangle}{\langle I(0)\rangle^2} = 1 + \exp(-2q^2Dt) \quad (2)$$

An example of an intensity correlation function of casein micelles is shown in Figure 2. Assuming homogeneous spherical particles, the apparent hydrodynamic radius R_H is derived from the Stokes−Einstein relation $D = k_B T/(6\pi\eta R_H)$, where k_B denotes the Boltzmann's constant and η the viscosity. In polydisperse systems, a distribution of relaxation times is required. On the basis of a cumulant expansion,[40] one determines the average diffusion coefficient from the initial slope of the intensity correlation function versus time. An example of such a fit using a cumulant expansion is shown for casein micelles in Figure 2 (solid line).

Figure 3 shows the resulting hydrodynamic radii (solid squares) as a function of the pH value of the casein solution. With increasing pH, the diameter of the casein micelles increases from 170 nm at pH of 5.5 to 480 nm at pH of 9.3. Other groups have observed a similar increase in micelle size with increasing pH. For example, Jusila et al.[41] observed a slight enlargement at pH larger than 7.4, Anema et al.[42] reported a rise in radius in the pH range from 6.5 to 7.1, and in the work of de Kruif et al.,[43] an increase in radius was stated as well. The interaction between the different caseins inside the micelle is balanced by repulsive electrostatic and attractive hydrophobic interactions.[13] The micelle formation is driven mostly by the hydrophobic interaction. At low Ca concentrations, the electrostatic repulsion limits the self-association and thus controls the size of the micelle. Within this model, a higher pH value results in a smaller net charge of the α- and β-caseins and thus an increased micelle size.[44−46] Independent of the selected pH, a large polydispersity was detected. It is known from literature that casein micelles

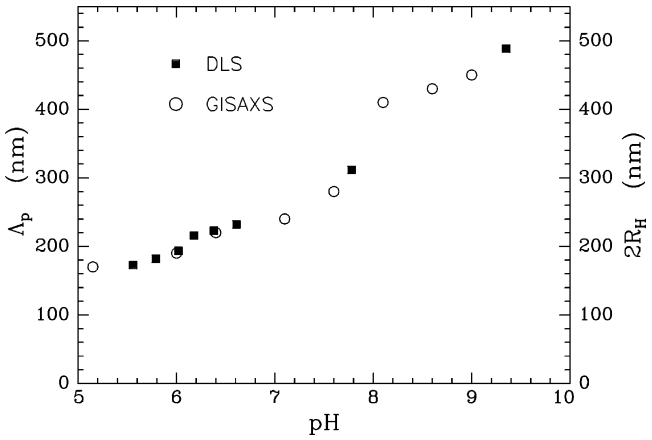

Figure 3. Influence of pH value on the size of the casein micelles in solution as probed by DLS revealing the hydrodynamic diameter $2R_H$ (filled squares). For comparison, the distance between neighboring micelles in dry casein films as probed with GISAXS corresponding to the most prominent in-plane length Λ_p (open circles) is shown.

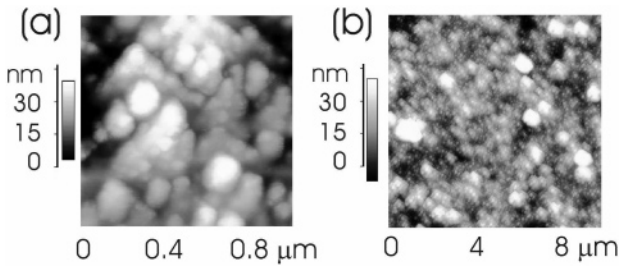

Figure 4. AFM images of the topography signal as measured with (a) 1 μm $\times$ 1 μm and (b) 10 μm $\times$ 10 μm scan range. The height scale is different for each pattern to depict the in-plane structure more clearly. For the presented example, thick casein films (concentration $c = 100$ g/L) at pH = 6.0 were probed.

are spherical and polydisperse particles with a mean diameter depending on key parameters such as pH.

In parallel with the hydrodynamic radius, the average light scattering intensity is increasing, suggesting an increase in average molecular weight of the micelles with pH. However, the average intensity depends not only on molecular weight, but also on polydispersity and the molecular form factor of the micelles. Thus, a quantitative evaluation of the static light scattering intensity is difficult and beyond the scope of this article.

For spin-coating, a high concentration of 100 g/L was selected to obtain thick films, which might exhibit a bulklike behavior, and to rule out typical thin film effects, e.g., introduced by the interaction with the glass substrate. With optical microscopy, the surface homogeneity was checked right after spin-coating. The pretreatment of the glass substrates with the base cleaning bath as described in the Experimental Section turned out to be essential for the creation of homogeneous films. The glass surface is hydrophilized and becomes wettable by the water-based casein solution.[47] Starting the spin-coating with an equally distributed solution is important for the preparation of homogeneous films. Without applying the base clean, the glass substrates as supplied from the manufacturer have a randomly defined surface chemistry, which depends strongly on the processing by the manufacturer. As a consequence, water might not wet or only partially wet the glass surface, and spin-coating results in inhomogeneous films.

Whereas optical microscopy is well-suited to examining lateral surface heterogeneities, with atomic force microscopy (AFM), the local surface structure is probed. Figure 4 shows typical examples of surface structures as measured with AFM. A representative high-resolution picture with 1 μm $\times$ 1 μm scan range is shown in Figure 4a. Spherical and polydisperse particles being identified as casein micelles are visible. The softer the samples are under investigation, the more the AFM probe compresses the material and only semiquantitative heights can be obtained.[48] If the scanning force had been too high, damage could have been induced in the internal structure (i.e., tip penetration in the sample, with irreversible breakage of material's integrity). For the presented data, the force regime was adjusted accordingly to leave the single casein micelles or their assemblies unaltered. Successive imaging was used for verification.[49] The typical assembly of the casein micelles is visualized in Figure 4b, exhibiting AFM data with 10 μm $\times$ 10 μm scan range. Beside polydisperse micelles with one mean diameter, a grainy-looking surface morphology is observed. It gives rise to a surface roughness of (11.1 $\pm$ 0.8) nm, which is larger than the value expected from the log-normal size distribution as determined with DLS. However, no preferential large-scale super structure is present, as observed with optical microscopy too, and therefore, we can conclude that a surface structure of type 1 (homogeneous surface, independent of position sample) is installed.

It should be noted that, in contrast to AFM on ultrathin films produced by solution casting,[48] the flat substrate is visible in the AFM data. The spherical gray−white colored particles represent casein micelles on top of a micrometer-thickness casein film. We do not compare the structural sizes obtained from AFM with the values resulting from DLS, because the statistical significance of both techniques differs by orders of magnitude. DLS gives averaged information, whereas AFM is a local probe only. Statistically more significant information on the casein films is obtained with grazing incidence small-angle X-ray scattering (GISAXS).

Furthermore, GISAXS probes the structure of the casein micelles inside the film in a nondestructive way. At the fixed angle of incidence of 0.6451°, the major scattering signals, namely, the specular and the Yoneda peak,[50] are well-separated on the detector and enable an easy detection of the GISAXS signal from the 2d intensity distribution via a horizontal cut. This horizontal slice contains only scattering contributions with an in-plane information. Because the flat glass surface gives no contribution with a marked intensity distribution to the diffuse scattering, the probed signal originated from the casein film only. The GISAXS experiments were performed with a very large sample−detector distance,[51] because the casein structure resulting from spin-coating is expected to exhibit characteristic lateral lengths above the resolution limit of a conventional small-angle scattering distance.

Figure 5 shows GISAXS cuts from the 2d intensity distribution measured at eight different pH values. In the typical double logarithmic presentation, the intensity is shown as a function of the q_y component of the scattering vector q. From the bottom to the top, the pH value increases (from 5.15 to 9.0). All GISAXS data have a characteristic rise of the intensity at very small q_y values close to the resolution limit (shown with the dashed line). This increase reveals the presence of unresolvable large-scale lengths describing the assembly of the casein micelles as visualized on the surface by AFM in Figure 4b. In addition, none of the GISAXS curves exhibit a well-pronounced peak in the intensity, in good agreement with the poydispersity of the casein micelles as probed by DLS. Instead of a peak, the GISAXS data are characterized by the presence of a shoulderlike intensity at low pH values. With increasing pH value, the position of the shoulder shifts toward smaller q_y values indicating

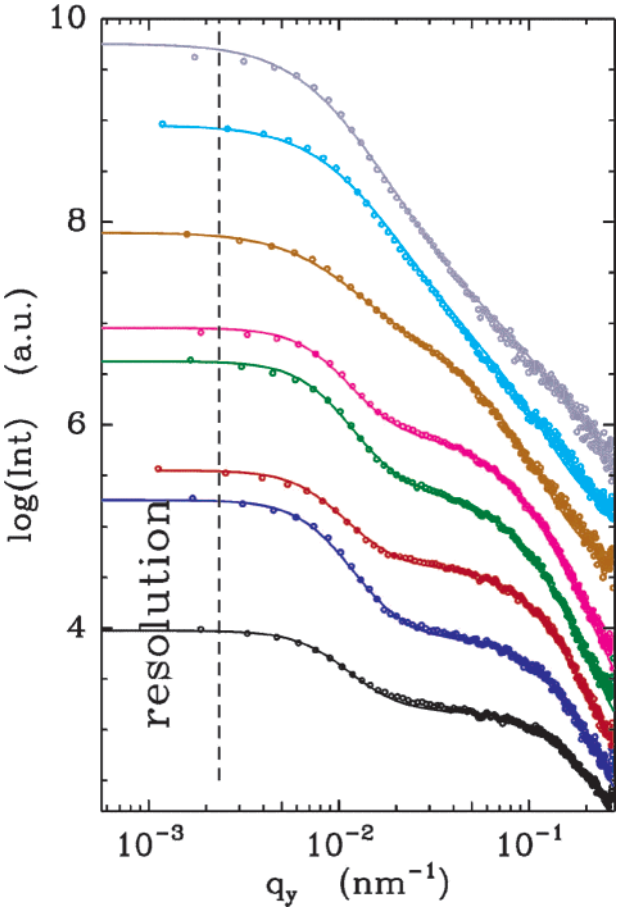

Figure 5. Double logarithmic plot of the GISAXS signal (dots) measured at thick casein films (concentration $c = 100$ g/L) prepared at different pH values together with model fits (solid lines) as explained in the text. From the bottom to the top, the pH increases (5.15, 6.0, 6.4, 7.1, 7.6, 8.1, 8.6, and 9.0). The curves are shifted along the *y*-axis for clarity. The resolution limit toward large length scales is shown by the dashed line.

an enlargement in the structural feature probed with GISAXS. For a quantitative description, the GISAXS data are fitted to a simple model.[52] The model is based on assuming a structure factorlike contribution resembling the distance between adjacent casein micelles. This distance, frequently called most prominent in-plane length Λ, is smeared by a Gaussian distribution. Because of the large polydispersity as probed by DLS, no special form factor was included. The experimental resolution is taken into account by a stretched Lorenzian-type distribution, as it was experimentally probed. The solid lines in Figure 5 show the best fits obtained within this model. The data are well-described within the entire probed q_y range. As a major result, the distance between adjacent casein micelles Λ is determined. Λ as a function of pH is plotted with open circles in Figure 3. With increasing pH value, it increases as well. In casein films prepared by a modified wet-spinning process, a strong influence of the pH of the film-forming solution on the film properties was reported.[53] At higher pH values, a denser ultrastructure was attributed to this influence.

The comparison of the hydrodynamic radii (Figure 3 shows the corresponding diameter), describing the mean micellar size in solution, with the most prominent in-plane length, describing the distance between neighboring casein micelles, is shown in Figure 3. We obtain a very good agreement of both values. The micelles are densely packed inside the film. Thus, the casein micelles are not disintegrated by spin-coating. Furthermore, the

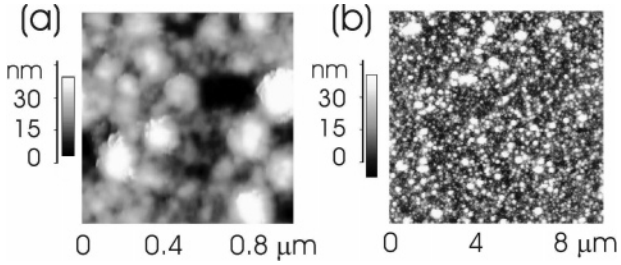

Figure 6. AFM images of the topography signal as measured with (a) 1 μm $\times$ 1 μm and (b) 10 μm $\times$ 10 μm scan range. The height scale is different for each pattern to depict the in-plane structure more clearly. For the presented example, casein films at pH = 8.1 prepared from a diluted solution with casein concentration $c = 10$ g/L were probed.

size of the micelles in the bulk film corresponds to the size of the micelles in solution, and no packing effects are observable. The polydispersity of the micelles prevents ordered packing and may account for the presence of additional long-range correlations not resolved by (high-resolution) GISAXS. However, GISAXS confirms the size enlargement of casein micelles with increasing pH value, as previously observed by photon correlation spectroscopy (PCS) in particle number frequency.

In contrast to our very good agreement, AFM carried out on casein films prepared with solution casting appears to give larger particle sizes than PCS on aqueous solutions.[48] Because solution casting resulted in ultrathin films, this experimental observation might be attributed to the film thickness, to the different preparation technique applied, or to the different substrate used (mica instead of glass).

2. Influence of Film Thickness on Structure. A variation in film thickness allows one to probe the crossover from a bulklike behavior to a thin film behavior. As known from synthetic polymers, in thin films the micelle morphology can be changed in comparison to the bulk. To address this topic, we not only compare one thin and one thick, bulklike film but present a full film thickness dependence which enables one to see the transition in more detail.

To focus on the effect of film thickness on the resulting casein micelle structures, the casein concentration used for spin-coating is varied. In DLS, no strong effect of the dilution on the determined casein micelle diameter was observed. From the spin-coating equation, a linear dependence between concentration and film thickness is installed.[17−19] Consequently, thinner casein films are prepared by diluting the water-based casein solution by the addition of purified buffer. Five different dilutions were chosen to reduce the film thickness by nearly 3 orders of magnitude. However, optical microscopy shows that inhomogeneous films result from the two most diluted solutions, and only at higher concentrations are homogeneous casein films installable. For this reason, the film thickness is no longer a well-defined parameter, and we take the concentration used for the spin-coating instead.

Again, AFM is used to picture the surface on a local scale. Figure 6 shows AFM data for a concentration $c = 10$ g/L. Spherical micelles and polydispersity of the micelles are visible on the small scan range of 1 μm $\times$ 1 μm in Figure 6a. Although perhaps not as established as in the case of thick films, Figure 6b reveals the presence of large-scale structures describing the micellar assembly. No bare glass surface area is detectable. The surface roughness is comparable to the case of thicker films with (10.8 $\pm$ 0.3) nm.

The improved statistical information is obtained from GISAXS. Figure 7 comprises GISAXS data of six different concentrations

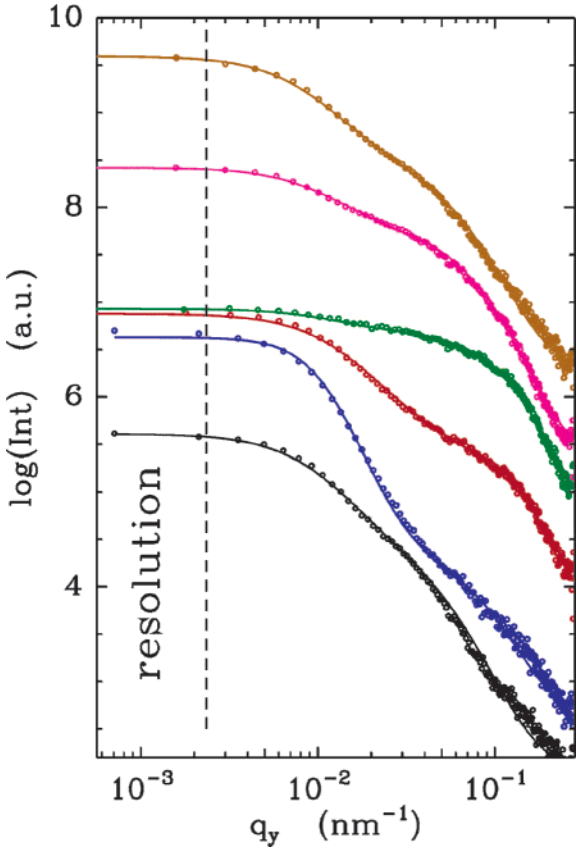

Figure 7. Double logarithmic plot of the GISAXS signal (dots) measured at casein films prepared at pH = 8.1 with different dilutions of the casein solution together with model fits (solid lines) as explained in the text. From the bottom to the top, the casein concentration increases (0.32, 1.0, 3.2, 10.0, 32.0, 100 g/L). The curves are shifted along the *y*-axis for clarity. The resolution limit toward large length scales is shown by the dashed line.

used for the spin-coating. From the bottom to the top, the concentration increases, and for comparison, the topmost curve belongs to the high concentration of 100 g/L used for the pH sample series discussed in the previous section. The general features are very comparable to the ones from Figure 5: At very small q_y values, the intensity rises due to unresolved large-scale structures and the distance between adjacent casein micelles is smeared by the polydispersity of the micelles. Therefore, the structure factor peak is more shoulderlike. Starting at the high concentration of 100 g/L, a dilution results in a shift of this shoulder toward larger q_y values corresponding to smaller real-space structures. This trend holds for the three dilution steps. Further dilution does not result in a thinner film, and the homogeneity is replaced with heterogeneity, best described as patches of casein film parts. In the GISAXS data, a turnover in the trend of the intensity shoulder is indicating that these patches consist of larger micelles again.

The solid lines in Figure 7 are model fits with the model introduced in the previous section. Again, the data are well-described by these fits. Slight deviations for the two bottom curves might result from the patchy surface structure which was not taken into account in the model. The most prominent in-plane length Λ_p, resulting from the fit and resembling the distance between adjacent micelles, is plotted in Figure 8 as a function of the concentration. For producible homogeneous casein films, the micelle size is reduced with decreasing film thickness. As a consequence, the diameter of the micelles is decreasing. So, in comparison to the size of the casein micelles

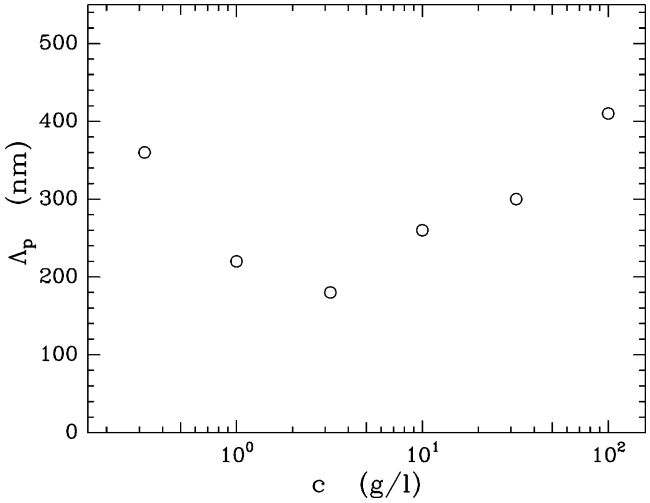

Figure 8. Influence of casein concentration of the water-based solution used for the spin-coating on the distance between neighboring micelles in dry casein films as probed with GISAXS corresponding to the most prominent in-plane length Λ_p (open circles).

in solution (given by the value at the highest concentration as explained in the previous section), in films with a reduced thickness the micelles are smaller. Reasons can be either a compression or a reorganization of the micelles in terms of the aggregation number. The smallest diameter determined is 180 nm. A comparable number was measured at very small pH values of pH ~5.

Figure 8 shows that the size of the micelles is not further decreased at very small concentrations. Instead of smaller micelles in a homogeneous film of reduced thickness, larger micelles are forming a heterogeneous patchy assembly. It is worth noting that all sizes of the micelles in solution are neither reached nor exceeded. Along this line, particle sizes larger than in bulk solutions (probed with PCS) are not explainable with film thickness effects. Thus, the interaction of caseins with the substrate, which is different for glass and mica, might be an explanation for the observation of larger micelles prepared by solution-casting on mica.[48]

However, solution-casting and spin-coating are completely different processes, with different forces acting on different time scales. Whereas in solution-casting the solvent evaporates slowly, spin-coating acts as a rapid quench. For a further discussion, shear fields introduced by the spin-coating are taken into account. Depending on the actual parameters applied during the spinning, a certain pressure is applied. Of course, it is impossible to experimentally measure this applied pressure, but an estimate results in a number on the order of 1 MPa.[54] From DLS experiments on diluted casein solution performed under pressure, the impact of pressure is known in the literature.[55−60] At moderate pressure, the micelles rearrange in a more compact size.[59] Thus, it is tempting to attribute the observed size decrease of the casein micelles to a similar effect.

With respect to the micellar size in solution, the more compact micelles are a nonequilibrium structure. The structure is trapped by the drying of the film. In the dry state, a relaxation into the equilibrium structure is not possible. Upon swelling in water or heating, a relaxation toward an equilibrium structure might become possible. As a consequence, swelling or heating experiments might be of interest for future research. It is important not to mix nonequilibrium with nonreproducibility. All presented structures can be reproduced by using spin-coating under exactly the same conditions. Changes in the casein

solution, the spinning parameters, or the pretreatment of the surfaces will change the obtained structures.

Summary

With spin-coating, a further technique for the preparation of thin casein films is added to the well-established solution-casting and spraying methods. Because it is a very powerful technique in the field of synthetic polymer film preparation, we newly introduce it in the field of casein films. A pretreatment of the glass substrates used for the spin-coating is a key part in the preparation. The applied base bath ensured wettability of the glass surface by the water-based casein solution. Thick homogeneous films resulted at high concentrations.

The casein micelles at the film surfaces are pictured in real space with AFM. For the structural investigation, an advanced X-ray scattering technique, namely, GISAXS, is utilized. Whereas AFM probes only the surface on a very limited area, GISAXS yields excellent sampling statistics. It averages over macroscopic regions to provide information on the nanometer scale. Thus, GISAXS enables the detection of statistically significant information. However, demanding very high resolution to probe structures in the range of casein micelles, GISAXS requires synchrotron radiation. Therefore, GISAXS experiments are rather demanding and not performable on a routine base.

With the pH value of the casein solution, a key parameter affecting the mean diameter of the casein micelles is addressed. In good agreement with the experimental observation using DLS, with increasing pH value the size also increases. A reduction in the electrostatic repulsion yields higher aggregation numbers of caseins and an enlargement in the micelle size.

While at high concentrations with spin-coating, bulklike films are prepared, whose structure matches well the micellar structure in solution (used for the spin-coating), at reduced concentrations, changes are observed. Comparable to the size reduction at moderate pressure, in thin casein films, the size of the micelles is reduced.

In summary, spin-coating is well-suited for the preparation of casein films. In contrast to the long times required for drying in the solution-casting technique, spin-coating is very quick. After 30 s only, a well-defined, homogeneous and dry film of very high quality is obtained. Besides the preparation of bulklike casein films, spin-coating allows for the preparation of nonequilibrium structures. As known from synthetic polymers as well, solution-casting yields structures close to equilibrium. Thus, spin-coating enlarges the range of producible structures as utilized in synthetic polymer films for years. In case of micellar casein films, nonequilibrium is established in the reduced size of the micelles forming the casein film.

Acknowledgment. We thank S. Cunis for the help during setting up the BW4 beamline at the HASYLAB. G. Schneider and T. Pöpperl helped during the GISAX experiments. We thank U. Kulozik for supplying the casein and for stimulating discussion. We obtain financial support by the BMBF (Förderkennzeichen 03CO333) and within the HASYLAB project II-03-025.

References and Notes

(1) Walstra, P.; Jenness, R. *Dairy Chemistry and Physics*; Wiley: New York, 1984.
(2) Holt, C.; de Kruif, C. G.; Tuinier, R.; Timmins, P. A. *Colloids Surf., A* **2003**, *213*, 275−284.
(3) Jöbstl, E.; O'Connell, J.; Fairclough, J. P. A.; Williamson, M. P. *Fibre Diffr. Rev.* **2004**, *12*, 66−69.
(4) Smyth, E.; Clegg, R. A.; Holt, C. *Int. J. Dairy Technol.* **2004**, *57*, 121−126.
(5) Holt, C.; Timmins, P. A.; Errington, N.; Leaver, J. *Eur. J. Biochem.* **1998**, *252*, 73−78.
(6) Pignon, F.; Belina, G.; Narayanan, T.; Paubel, X.; Magnin, A.; Gesan-Guiziou, G. *J. Chem. Phys.* **2004**, *121*, 8138.
(7) Kalnin, D.; Quennesson, P.; Artzner, F.; Schafer, O.; Narayanan, T.; Ollivon, M. *Prog. Colloid Polym. Sci.* **2004**, *126*, 139−145.
(8) Malin, E. L.; Alaimo, M. H.; Brown, E. M.; Aramini, J. M.; Germann, M. W.; Farrell, H. M.; McSweeney, P. L. H.; Fox, P. F. *J. Protein Chem.* **2001**, *20*, 391−404.
(9) McMahon, D. J.; McManus, W. R. *J. Dairy Sci.* **1998**, *81*, 2985−2993.
(10) Walstra, P. *Int. Dairy J.* **1999**, 189−192.
(11) Schmidt, D. G. *Developments in Dairy Chemistry-1*; Elsevier Applied Science: London, 1982; pp 61−86.
(12) Schmidt, D. G.; Walstra, P.; Buchheim, W. *Neth. Milk Dairy J.* **1973**, *27*, 128−142.
(13) Horne, D. S. *Int. Dairy J.* **1998**, *8*, 171−177.
(14) Horne, D. S. *Colloids Surf., A* **2003**, *213*, 255−263.
(15) Bauer, R.; Hansen, M.; Hansen, S.; Oegendal, L.; Lomholt, S.; Qvist, K.; Horne, D. *J. Chem. Phys.* **1995**, *103*, 2725−2737.
(16) Avena-Bustillos, R. J.; Krochta, J. M. *J. Food Sci.* **1993**, *58*, 904−907.
(17) Lawrence, C. J. *Phys. Fluids* **1988**, *31*, 2786.
(18) Spangler, L. L.; Torkelson, M.; Royal, J. S. *Polym. Eng. Sci.* **1990**, *30*, 644.
(19) Schubert, D. W. *Polym. Bull.* **1997**, *38*, 177.
(20) Müller-Buschbaum, P.; Stamm, M. *Macromolecules* **1998**, *31*, 3686.
(21) Emslie, A. G.; Bonner, F. T.; Peck, L. G. *J. Appl. Phys.* **1958**, *29*, 858.
(22) Bornside, D. E.; Macosko, C. W.; Scriven, L. E. *J. Electrochem. Soc.* **1991**, *138*, 317.
(23) Anema, S. G.; Lowe, E. K.; Lee, S. K. *Lebensm. Wiss. Technol.* **2004**, *37*, 779−787.
(24) Jussila, M. A.; Yohannes, G.; Riekkola, M. L. *J. Microcolumn Sep.* **1997**, *9*, 601−609.
(25) de Kruif, C. G. *J. Dairy Sci.* **1998**, *81*, 3019−3028.
(26) Tolkach, A.; Kulozik, U. *J. Food Eng.* **2005**, *67*, 13−20.
(27) Salditt, T.; Metzger, T. H.; Peisl, J.; Reinker, B.; Moske, M.; Samwer, K. *Europhys. Lett.* **1995**, *32*, 331.
(28) Naudon, A.; Babonneau, D.; Thiaudiere, D.; Lequien, S. *Physica B* **2000**, *283*, 69.
(29) Müller-Buschbaum, P. *Ann. Bioanal. Chem.* **2003**, *376*, 3.
(30) Gehrke, R. *Rev. Sci. Instrum.* **1992**, *63*, 455.
(31) Tolan, M. *X-ray scattering from soft-matter thin films*; Springer-Verlag: Berlin, 1999.
(32) Hol, V.; Baumbach, T. *Phys. Rev. B* **1994**, *49*, 10668.
(33) Müller-Buschbaum, P.; Gutmann, J. S.; Stamm, M. *J. Macromol. Sci., B* **1999**, *38*, 577.
(34) Geoghegan, M.; Krausch, G. *Prog. Polym. Sci.* **2003**, *28*, 261.
(35) Müller-Buschbaum, P.; Bauer, E.; Wunnicke, O.; Stamm, M. *J. Phys.: Condens. Matter* **2005**, *17*, S363−S386.
(36) Müller-Buschbaum, P.; Gutmann, J. S.; Wolkenhauer, M.; Kraus, J.; Stamm, M.; Smilgies, D.; Petry, W. *Macromolecules* **2001**, *34*, 1369.
(37) Müller-Buschbaum, P.; Hermsdorf, N.; Roth, S. V.; Wiedersich, J.; Cunis, S.; Gehrke, R. *Spectrochim. Acta, Part B* **2004**, *59*, 1789.
(38) Walstra, P. *J. Dairy Sci.* **1990**, *73*, 1965−1979.
(39) Berne, B.; Pecora, R. *Dynamic Light Scattering*; Wiley: New York, 1976.
(40) Koppel, D. *J. Chem. Phys.* **1972**, *57*, 4814−4820.
(41) Jussila, M. A.; Yohannes, G.; Riekkola, M. L. *J. Microcolumn Sep.* **1997**, *9*, 601−609.
(42) Anema, S. G.; Lowe, E. K.; Lee, S. K. *Lebensm. Wiss. Technol.* **2004**, *37*, 779−787.
(43) de Kruif, C. G. *J. Dairy Sci.* **1998**, *81*, 3019−3028.
(44) Payens, T. A.; Brinkhuis, J. A.; van Markwijk, B. W. *Biochim. Biophys. Acta* **1969**, *175*, 434−437.
(45) Schmidt, D. G. *Biochim. Biophys. Acta* **1970**, *207*, 130−138.
(46) Schmidt, D. G. *Biochim. Biophys. Acta* **1970**, *221*, 140−141.
(47) Müller-Buschbaum, P. *Eur. Phys. J. E* **2003**, *12*, 443.
(48) Regnault, S.; Thiebaud, M.; Dumay, E.; Cheftel, J. C. *Int. Dairy J.* **2004**, *14*, 55−68.
(49) Uricanu, V. I.; Duits, M. H. G.; Mellema, J. *Langmuir* **2004**, *20*, 5079−5090.

(50) Yoneda, Y. *Phys. Rev.* **1963**, *131*, 2010.
(51) Müller-Buschbaum, P.; Casagrande, M.; Gutmann, J.; Kuhlmann, T.; Stamm, M.; Cunis, S.; von Krosigk, G.; Lode, U.; Gehrke, R. *Europhys. Lett.* **1998**, *42*, 517.
(52) Panagiotou, P.; Bauer, E.; Loi, S.; Titz, T.; Maurer, E.; Müller-Buschbaum, P. *Z. Kristallogr.* **2004**, *219*, 210−217.
(53) Finault, A.; Gallant, D. J.; Bouchet, B.; Dumont, J. P. *J. Food Sci.* **1997**, *62*, 744−747.
(54) Reiter, G. *Eur. Phys. J. E* **2002**, *8*, 251−255.
(55) Desobry-Banon, S.; Richard, F.; Hardy, J. *J. Dairy Sci.* **1994**, *77*, 3267−3274.
(56) Anema, S. G.; Lee, S. K.; Schrader, K.; Buchheim, W. *Milchwissenschaft* **1997**, *52*, 141−146.
(57) Needs, E. C.; Stenning, R. A.; Gill, A. L,; Ferragut, V.; Rich, G. T. *J. Dairy Res.* **2000**, *67*, 31−42.
(58) Gebhardt, R.; Doster, W.; Kulozik, U. *Braz. J. Med. Biol. Res.* **2005**, *38*, 1209−1214.
(59) Gebhardt, R. Ph.D. Thesis, TU Munich, Munich, Germany, 2005.
(60) Gebhardt, R.; Doster, W.; Friedrich, J.; Kulozik, U. *Eur. Biophys. J.* In press.

BM060088U